CRYSTAL GROWTH & DESIGN
2006
VOL. 6, NO. 4
892−898

Direct Design of Pharmaceutical Antisolvent Crystallization through Concentration Control

George X. Zhou,[†] Mitsuko Fujiwara,[‡] Xing Yi Woo,[‡,§] Effendi Rusli,[‡] Hsien-Hsin Tung,[†] Cindy Starbuck,[†] Omar Davidson,[†] Zhihong Ge,[†] and Richard D. Braatz*[,‡]

Merck & Co., Inc., 126 East Lincoln Ave., P.O. Box 2000, Rahway, New Jersey 07065, Department of Chemical and Biomolecular Engineering, University of Illinois at Urbana−Champaign, 600 South Mathews Avenue, Urbana, Illinois 61801, and Department of Chemical and Biomolecular Engineering, National University of Singapore, 4 Engineering Drive 4, Singapore 117576

Received August 10, 2005; Revised Manuscript Received January 23, 2006

ABSTRACT: Recent advances in in situ measurement technology and automation of batch crystallizers have enabled the development of batch crystallization recipes in which the desired supersaturation profile is followed by feedback control. This paper describes a new approach for following supersaturation setpoints for antisolvent crystallizations that is easy to implement for the tried crystallization. Simulations and application to a proprietary drug compound demonstrate how this combination of automation and in process measurements enables the rapid development of batch crystallization processes in the pharmaceutical industry.

1. Introduction

Increasing emphasis is being placed on designing and operating pharmaceutical crystallization processes to produce a consistent crystal product.[1] In industry, the batch crystallization recipe is usually designed to follow a temperature or antisolvent addition profile. Rigorous determination of an optimal batch recipe requires accurate growth and nucleation kinetics, which can be determined in a series of continuous or batch experiments.[2−4] For aggregating and other complex crystallization systems, it can be time consuming to construct models and determine kinetics that are accurate enough to compute an optimal batch recipe. This has resulted in the common industrial practice of trial-and-error experimentation to design batch recipes for pharmaceutical crystallization. An alternative approach that does not require accurate kinetics or trial-and-error experimentation is to control the crystallizer so that it follows a supersaturation profile in the metastable zone based on concentration measurement.[5−8] The advantage of this approach is its low sensitivities to most practical disturbances and to variations in the nucleation and growth kinetics and that this method does not require the extra time needed for the determination of crystallization kinetics.[9]

This paper describes a concentration control system and its application to following setpoint supersaturation profiles in the metastable zone for batch antisolvent crystallization. This extends past studies in cooling crystallization, in which automated systems[5,8,10] were implemented that determine the metastable limit and the solubility curve from in situ laser backscattering (Lasentec FBRM)[5,8,11] or attenuated total reflection Fourier transform infrared (ATR-FTIR) spectroscopy.[5,12−16] In the concentration control systems, the supersaturation is calculated from the in process solution concentration measurement (using ATR-FTIR spectroscopy) and the previously measured solubility curve. In antisolvent crystallization, the crystallizer follows setpoint supersaturation profiles by adjusting the addition rate (see Figure 1).

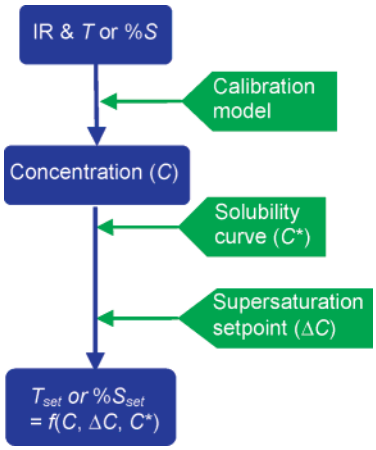

Figure 1. Schematic of concentration control. Solution concentration is estimated from IR absorbances and temperature (for cooling crystallization) or % solvent (for antisolvent crystallization) using the calibration model. The next temperature or % solvent setpoint is calculated from the concentration, solubility, and user-defined supersaturation setpoint.

This paper describes an approach for the concentration control of antisolvent crystallization, which is implemented so that the antisolvent addition rate is an algebraic function of the supersaturation defined by the setpoint profile. The implementation in Visual Basic was designed so that the metastable zone determination and batch recipe design can be operated in an automated manner while providing a graphical user interface so that the user can make adjustments based on level of expertise. Application of the automated system to a proprietary drug compound enabled the rapid testing of various supersaturation profiles, which indicated that following a constant relative supersaturation profile, rather than a constant supersaturation profile, resulted in reduced secondary nucleation without compromising batch time for the particular crystallization system studied here. This study demonstrates how this combination of automation and in process measurements enables the rapid development of crystallization processes in the pharmaceutical industry. A preliminary (i.e., less automated) version of the methodology described here was implemented on the antisolvent crystallization of paracetamol (acetaminophen) from acetone−water.[17]

* Corresponding author. Phone: 217-333-5073. Fax: 217-333-5052. E-mail: braatz@uiuc.edu.
[†] Merck & Co., Inc.
[‡] University of Illinois at Urbana−Champaign.
[§] National University of Singapore.

10.1021/cg0504049 CCC: $33.50
Published on Web 02/25/2006

2. Theory

The previously published methods for operating cooling crystallization, which use PI control[5] or cascade control,[8] require tuning of feedback controller parameters, whose values depend strongly on the unknown crystallization kinetics, to follow the setpoint supersaturation. An approach that does not require controller tuning, except at a lower level to track the reactor temperature or antisolvent addition rate, is described here. A commercially available circulator bath and a syringe pump were used in this study, which had the capability to track setpoint temperature and pump rate, respectively. The setpoint is in terms of the supersaturation defined as $\Delta c = c - c^*$, where c is the solution concentration and c^* is the solubility, although the approach also can be applied to any other supersaturation definition (e.g., defined in terms of activities or relative concentrations). Replacing the measured solution concentration c_{meas} for c and an algebraic function for the solubility as a function of temperature T for c^* gives

$$c^*(T) = c_{meas} - \Delta c \quad (1)$$

Solving this equation for T gives the temperature setpoint. The successful implementation of this approach on a cooling crystallization of a proprietary pharmaceutical compound to follow a constant supersaturation profile is shown in Figure 2. The simplest extension of this approach to antisolvent crystallization is obtained by substituting T with % solvent (%S, solute-free basis):

$$c^*(\%S) = c_{meas} - \Delta c \quad (2)$$

The antisolvent addition rate is calculated by solving the equation for the % solvent setpoint, %S. This equation can be improved by taking the effect of dilution into account:

$$c^*(\%S) = (\%S/100)(m_{solute}/S) - \Delta c \quad (3)$$

where m_{solute} is the mass of solute and S is the mass or volume of solvent.

Figure 1 is a schematic of the concentration control implementation. A control engineer would refer to this approach as nonlinear state feedback control,[18] because the controller determines the value for the manipulated variable based on a nonlinear function (eqs 1, 2, or 3) of the measurement of a process state. Although the control eqs 1−3 have no tuning parameters and are functions of only the solubility curve and the supersaturation setpoint, it is seen below that the approach leads to fast setpoint tracking. While most process control systems have their setpoints specified as an explicit function of time,[19] this is not true for the above control implementation. The speed at which the process moves along the supersaturation setpoint trajectory (e.g., see top plot in Figure 2) and the total batch time are determined by the crystallization kinetics.

Small errors in the concentration measurement, c_{meas}, or the expression for the solubility, c^*, result in small errors in the implemented supersaturation, Δc, due to the relationships between the variables in eqs 1−3. More specifically, with errors in c^* and c_{meas}, the true implemented supersaturation can be computed from eq 1:

$$c^* = c^*_{true} + \epsilon_{c^*} = c_{meas} - \Delta c_{desired} = (c_{true} + \epsilon_c) - \Delta c_{desired} \rightarrow \Delta c_{true} \equiv c_{true} - c^*_{true} = \Delta c_{desired} - \epsilon_c + \epsilon_{c^*} \quad (4)$$

Hence errors in c^* and c_{meas} have the same magnitude effect on the implemented supersaturation. Such small errors in the supersaturation affect the relative rates of crystallization processes, resulting in some variation in the crystal size distribution and the total batch time.

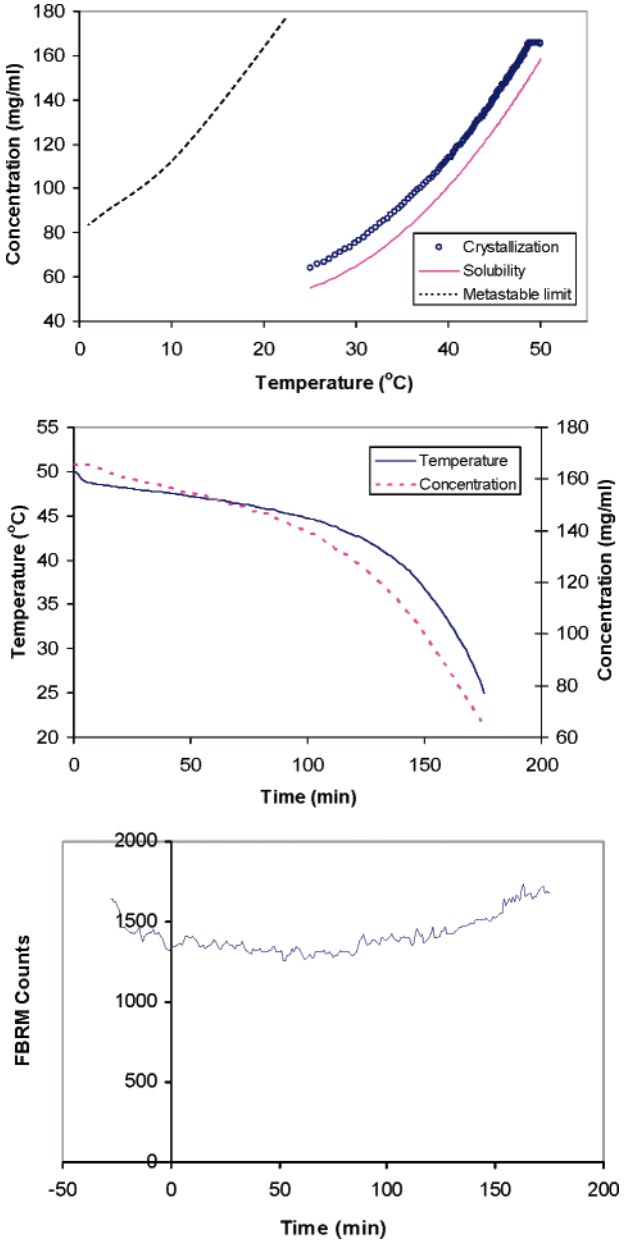

Figure 2. The concentration−temperature profile (top) and the corresponding time profiles for concentration, temperature (middle), and FBRM counts (bottom) during the seeded cooling crystallization of a pharmaceutical compound using a constant supersaturation setpoint ($\Delta c = 10$ mg/mL$_{solvent}$). The metastable limit was measured at a cooling rate of 0.4 °C/min. The time of 0 min is defined as the start of concentration control.

An alternative interpretation of the control scheme in Figure 1 is that eqs 1−3 merely provide a setpoint to a lower level controller that tracks the reactor temperature or antisolvent addition rate. Commercially available circulator baths, such as that used in this study, have a pretuned embedded feedback controller that stably follows a user-specified temperature. Similarly, commercially available syringe pumps such as that used in this study stably follow a user-specified pump rate.

The approach taken in this manuscript can quickly determine near-optimal supersaturation trajectories. Several papers argue that constant supersaturation profiles are close to optimal for many crystallization systems,[20−22] which suggests the initial

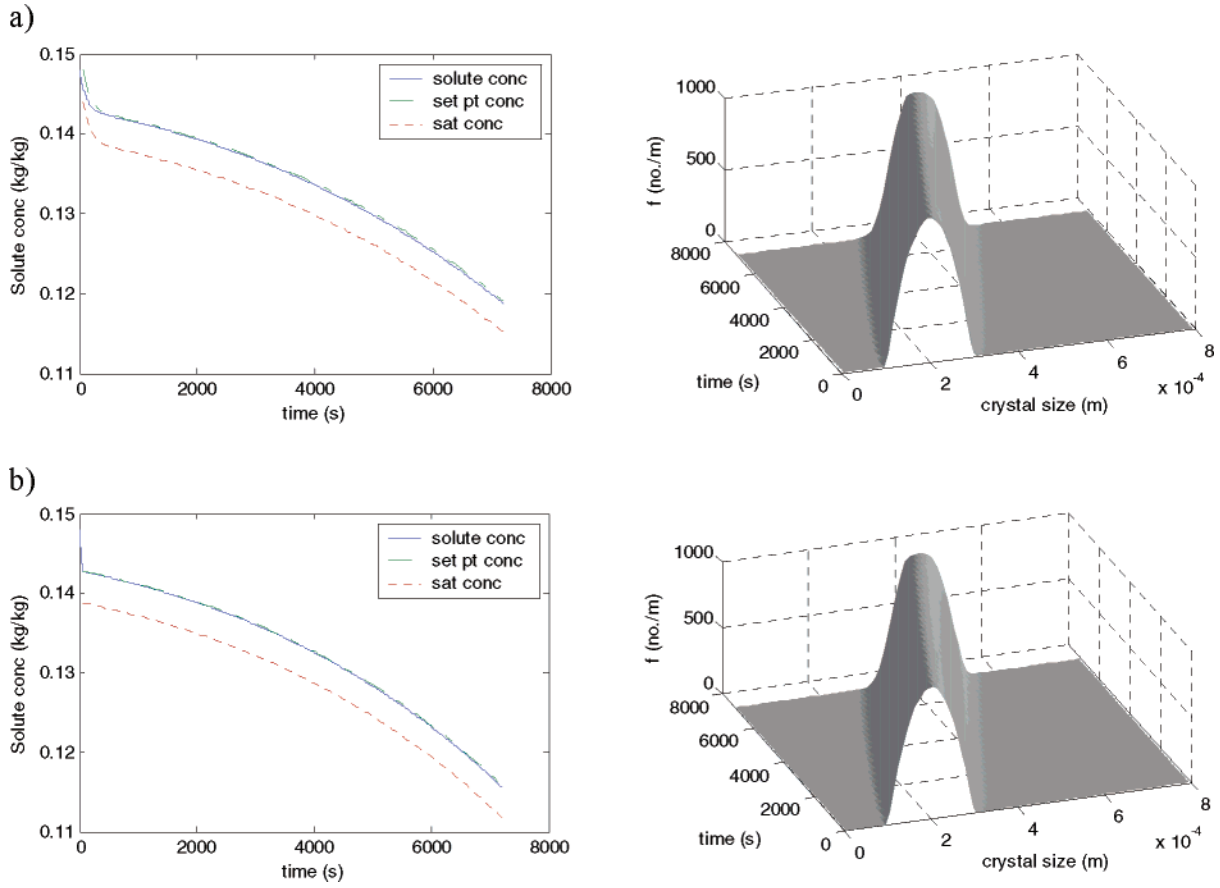

Figure 3. The supersaturation profiles and product crystal size distributions during the simulated seeded antisolvent crystallization of paracetamol in acetone−water mixture. Results from eq 2, which ignores the dilution effect (a), and eq 3, which considers dilution effect (b), are compared. The simulation uses a sampling time $t_s = 60$ s, a constant supersaturation setpoint $\Delta c = 0.004$ $kg_{solute}/kg_{water+acetone}$, and a seed amount of 1.586 $g/kg_{water+acetone}$ over a batch time of 2 h.

operation of the batch crystallizer for various constant values of the supersaturation. Without extensive modeling studies, it is not possible to determine a priori the *optimal* supersaturation profile for a particular complex crystallization process; however, analysis of the experimental data obtained from constant-supersaturation trajectories can be used to move toward trajectories that are closer to optimality. A nearly optimal trajectory can be reached more quickly by using several crystallizers in parallel (e.g., via the MultiMax Art 1250, Mettler Toledo, Inc., Columbus, OH).

The implementation of eqs 2 and 3 in simulations of the antisolvent crystallization of paracetamol in an acetone−water mixture is shown in Figure 3 (see Appendix for details on the simulation model and experimentally determined kinetic parameters and solubility). Equation 3, which considers the effect of dilution, follows the supersaturation setpoint profile more closely (see Figure 3) and hence was implemented on the antisolvent crystallization of the proprietary pharmaceutical compound described in the next section. Note that in practice the difference may not be noticeable depending on the extent of measurement noise.

3. Experimental Methods

The temperature of the crystallizer was controlled with a Pt100 thermocouple connected to a circulator bath (Haake F8). The solvent and the antisolvent were added by programmable syringe pumps (Harvard Apparatus PHD 4400). ReactIR 4000 software (Mettler Toledo, version 3.0) was used to collect the ATR-FTIR spectra every minute. The calibration model relating the spectra and % solvent to in situ solution concentration was constructed by using partial least-squares (PLS) and various principal component regression (PCR) methods applied to mean-centered normalized experimental data.[15,16] Fifty percent of the experimental data were used for calibration, and 50% of the data were used for validation, following the procedure described in ref 16. The Matlab implementations of PLS and the PCR methods were validated by comparison to calibration models obtained by Unscrambler (CAMO, Inc.). Solution turbidity was measured every 5 s with Lasentec FBRM (Mettler Toledo) for counts in the 10−50 μm size range. The graphical user interface for the automation of data collection, solubility measurement, and concentration control was written in Microsoft Visual Basic 6.0. The Visual Basic interface calls a program[15,16] written in Matlab (The MathWorks, Inc.) for calibration model development using chemometrics and calls the Matlab program *roots* to obtain solutions to eqs 1 and 3 for polynomial functions c^*. Figure 4 shows the schematic of the apparatus and instrument setup. The solvent was toluene, and the antisolvent was *n*-heptane. For isothermal batch antisolvent crystallizations, the initial solvent volumes were 123−125 mL (100% solvent), depending on the batch, and the seed crystals were aged for ∼1 h before antisolvent addition.

4. Results and Discussion

4.1. Calibration and Solubility. ATR-FTIR spectroscopy has been used for in situ concentration measurement during antisolvent crystallizations.[23,24] To reduce the time and labor for data collection for the calibration of IR spectra to concentration, an automated method was developed. The IR spectra for calibration were collected automatically by sequentially adding the antisolvent and solvent to the initial solution to cover a range of concentration and solvent−antisolvent ratio (see Figure 5). The endpoints for antisolvent and solvent additions are based

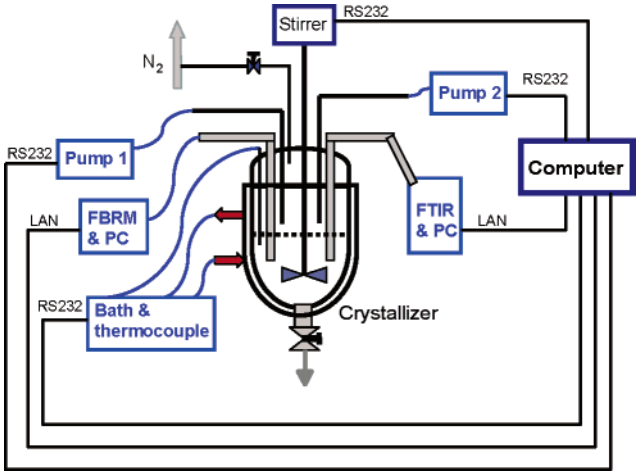

Figure 4. Schematic of the apparatus and instrument setup used for antisolvent crystallization.

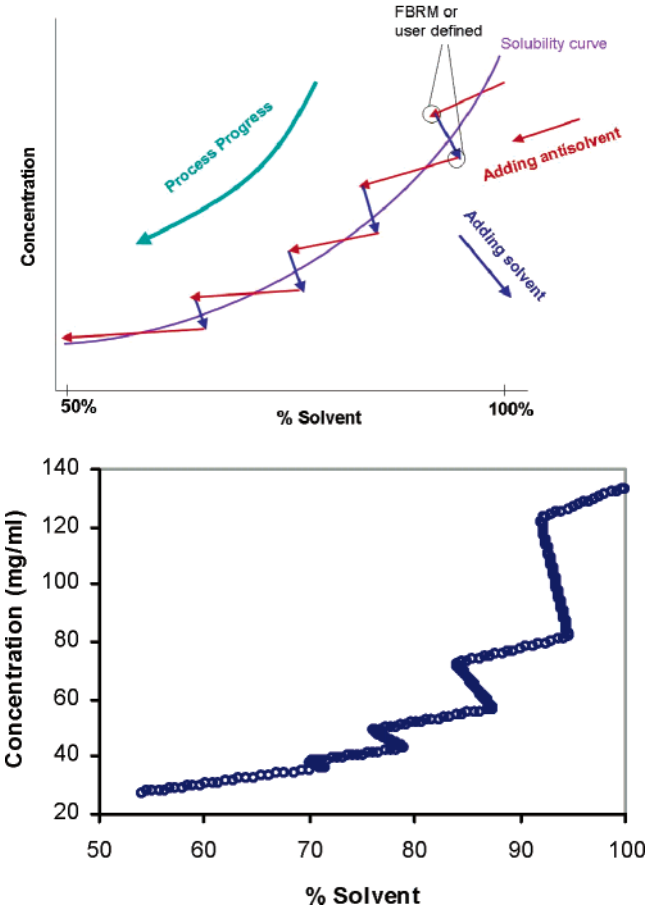

Figure 5. The path of concentration vs % solvent for collecting the IR spectra for constructing the calibration model: schematic (top) and experimental results (bottom). The unit for concentration is $mg_{solute}/mL_{solvent+antisolvent}$.

on data from the FBRM or a combination of user-defined target values and FBRM data, depending on the extent of the user's prior knowledge of the crystallization system. IR spectra were collected while the solution remained clear based on FBRM data (i.e., while particle counts were below a user-specified threshold value). During the antisolvent addition stage, the metastable limit can be detected by an increase in FBRM counts, which indicates nucleation. For this study, the user-defined target

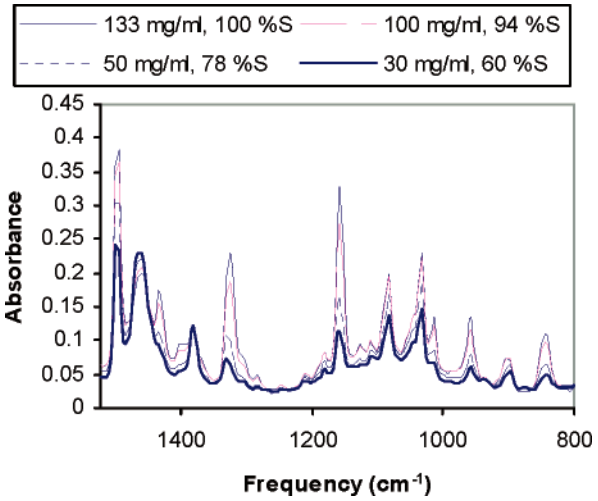

Figure 6. Sample IR spectra at various concentrations and solvent−antisolvent ratios for a pharmaceutical compound.

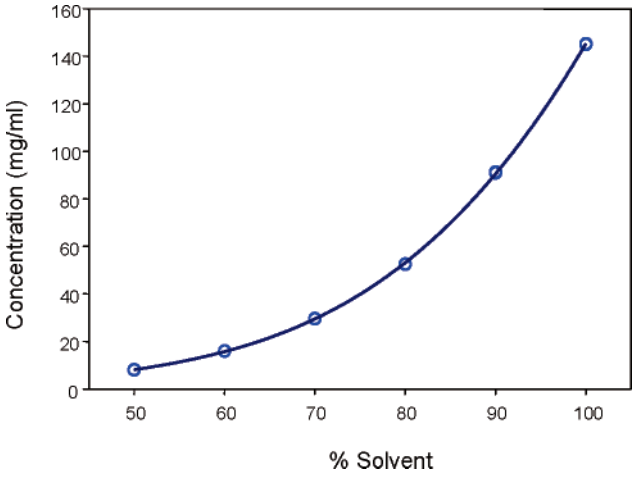

Figure 7. Solubility of the pharmaceutical compound at 50 °C for various solvent−antisolvent ratios.

values were such that the operations were completely within the metastable zone, and the metastable limit was not detected.

The IR spectral frequency range 799−1524 cm^{-1} was used to build the calibration model relating ATR-FTIR spectra to solution concentration (see Figure 6). Temperature was not incorporated into the calibration model because it remained constant at 50 °C. A PLS model with standard error of cross validation (SECV) of 0.3 mg/mL and prediction interval of 1.1 mg/mL was selected. The number of principal components used for this model was 7. The solubility of the pharmaceutical compound at 50 °C was determined from the calibration model and the IR spectra of the slurry equilibrated at various solvent−antisolvent ratios (see Figure 7). The solubility data were fit to a cubic function of % solvent (%*S*).

4.2. Concentration Control. Seeded antisolvent crystallizations were carried out using the concentration control eq 3 to follow various supersaturation profiles. A range of constant supersaturation profiles (Δc = 10, 20, and 30 mg/mL) were investigated (see Figure 8). The antisolvent addition rate increases as the crystallization progresses (see Figure 9) due to increase in the crystal surface area as expected from previous results.[25] This is similar to cooling crystallization, where the cooling rate increases as the crystallization progresses (see Figure 2). For the antisolvent crystallization following Δc = 10 mg/mL, there was a disturbance in the concentration

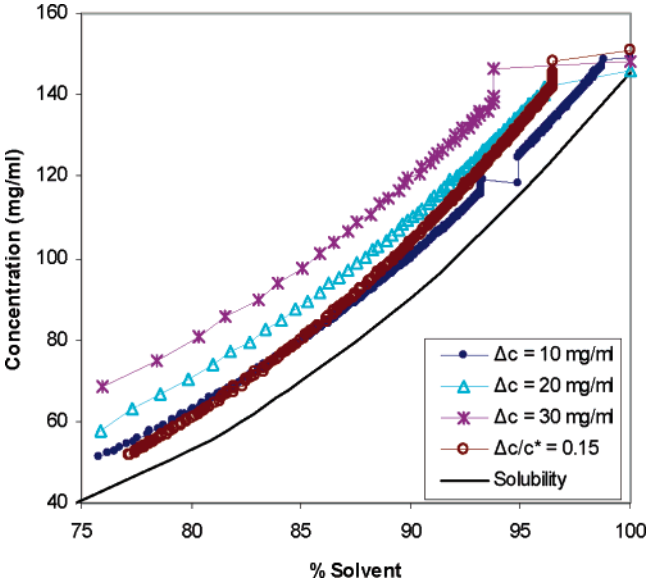

Figure 8. Various supersaturation profiles (Δc = 10, 20, and 30 mg/mL$_{solvent+antisolvent}$, $\Delta c/c^*$ = 0.15) followed during the seeded antisolvent crystallization of a pharmaceutical compound from a mixture of toluene and *n*-heptane with 3% seed loading.

measurement that occurred around 330 min at 94% solvent from which the system recovered. Unlike cooling crystallization where the temperature can move up or down depending on the concentration, a crystallization setup in which only antisolvent can be added cannot move to a higher % solvent setpoint. This limits the response of the system to suppressing some disturbances. The system can be easily programmed so that both solvent and antisolvent can be added during crystallization, the drawback being an increase in the total amount of dilution that occurs during the batch crystallization.

Higher constant supersaturations (Δc = 20 and 30 mg/mL) resulted in shorter batch times with excessive secondary nucleation (see Figure 10). This excessive secondary nucleation (compared to Δc = 10 mg/mL) is consistent with nucleation theory, which indicates that the nucleation rate is a strong monotonic function of the supersaturation.[28] Because secondary nucleation increases with crystal mass,[28] the secondary nucleation rate increases as the crystallization proceeds at constant absolute supersaturation. The use of a constant relative supersaturation $\Delta c/c^*$ setpoint was motivated by the idea that decreasing the absolute supersaturation Δc during the batch would compensate for the effect of increased crystal mass on the secondary nucleation rate to reduce excessive secondary nucleation.

As shown in Figure 10, secondary nucleation was not observed with a constant relative supersaturation, $\Delta c/c^*$ = 0.15, which had Δc = 22 mg/mL at the beginning of the run that decreases to Δc < 10 mg/mL as the crystallization progresses (see Figure 8). The absolute supersaturation Δc decreased sufficiently fast during the batch to avoid significant secondary nucleation, and for a similar value for the final Δc, the crystallization starts at higher Δc, which reduced the batch time compared to supersaturation profile Δc = 10 mg/mL.

For the antisolvent system studied here, following a constant relative supersaturation was a better strategy than following a constant supersaturation. Constant relative supersaturation resulted in less secondary nucleation compared to following constant supersaturation (see Figure 10). The disadvantage of using relative supersaturation is that any error in the concentration measurement is amplified as the crystallization progresses since c^* becomes small.[8] Other possible methods to reduce secondary nucleation include heating the antisolvent, which requires modification in the experimental setup, and the use of a mixture of solvent and antisolvent in place of the antisolvent, which results in extra dilution of the system.

The concentration control approach described here demonstrates an automated approach for the systematic investigation of different supersaturation profiles in the search for optimal

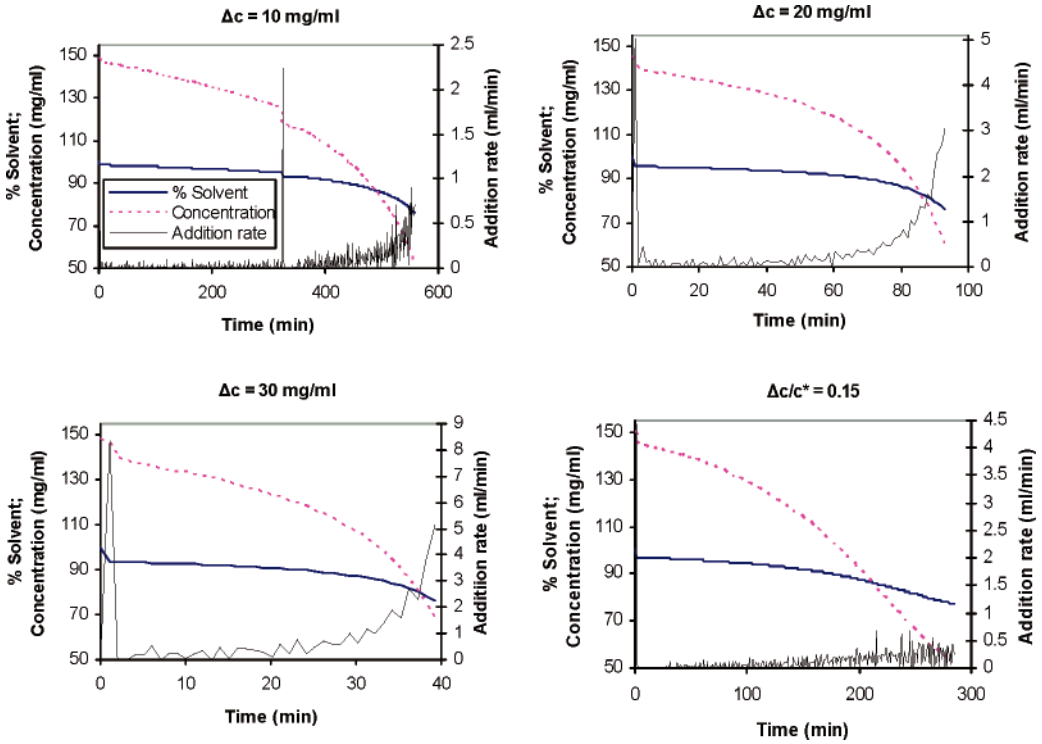

Figure 9. The % solvent, concentration, and addition rate profiles over time for the various supersaturations (Δc = 10, 20, and 30 mg/mL$_{solvent+antisolvent}$, $\Delta c/c^*$ = 0.15) followed during the seeded antisolvent crystallization of a pharmaceutical compound from toluene−*n*-heptane mixture.

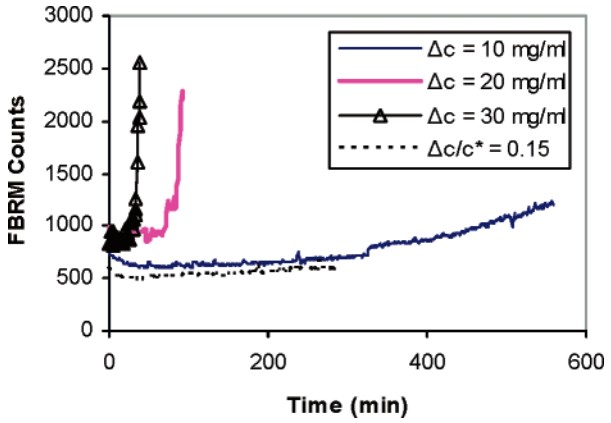

Figure 10. FBRM counts in the 10−50 μm range over time for Δc = 10, 20, and 30 mg/mL$_{solvent+antisolvent}$ and $\Delta c/c^* = 0.15$ during the seeded antisolvent crystallization of a pharmaceutical compound from toluene−*n*-heptane mixture.

antisolvent addition rate profiles. This enables promising batch recipes to be quickly identified for optimizing various product crystal properties such as crystal size distribution, crystal shape, and polymorphism—reducing the overall time for process development.

Acknowledgment. Merck & Co., Inc. is acknowledged for their financial support of this project. We also thank Christina Jackson for her assistance in collecting valuable data for the development of the program.

Appendix: Simulation Model for the Paracetamol−Water−Acetone System

The nucleation and growth kinetics and the solubility curve for the paracetamol−water−acetone system were estimated from the experimental results of Granberg et al.:[26,27]

$$B = 8.560\,80 \times 10^8 \exp\left[-1.228\,50 \times 10^{-3}\frac{(\ln(c_s/c^*\,(\mathrm{kg/m^3})))^3}{(\ln(c/c^*))^2}\right] \quad \text{(A1)}$$

$$G = k_g \Delta c^g, \qquad \Delta c = c - c^* \quad \text{(A2)}$$

$$k_g = 4.010\,67 \times 10^8 w^2 - 1.761\,98 \times 10^{-6} w + 5.781\,35 \times 10^{-5} \quad (w > 30\%) \quad \text{(A3)}$$

$$g = -4.225\,36 \times 10^{-3} w + 1.774\,28 \quad (w > 30\%) \quad \text{(A4)}$$

$$c^* = -5.019\,02 \times 10^{-12} w^6 + 1.697\,67 \times 10^{-9} w^5 - 2.467\,65 \times 10^{-7} w^4 + 2.192\,62 \times 10^{-5} w^3 - 1.270\,18 \times 10^{-3} w^2 + 3.426\,14 \times 10^{-2} w + 7.960\,86 \times 10^{-2} \quad \text{(A5)}$$

where B = nucleation rate (no. of particles/s·m^3), G = growth rate (m/s), c_s = solid crystal density (1293 kg/m^3), c^* = saturation concentration (kg$_{paracetamol}$/kg$_{water+acetone}$), c = solute concentration (kg$_{paracetamol}$/kg$_{water+acetone}$), and w = antisolvent mass % on a solute-free basis.

The well-mixed batch crystallization was modeled by the population balance equation:[28,29]

$$\frac{\partial f}{\partial t} + \frac{\partial [Gf]}{\partial r} = B\delta(r - r_0) \quad \text{(A6)}$$

where the particle number density function (f) is a function of the crystal size (r) and time (t), r_0 is the size of a nucleated crystal, and δ is the Dirac delta function. Equation A6, rewritten on a mass basis, was solved by a high-resolution finite-volume semidiscrete central scheme:[30]

$$\frac{d}{dt} f_{w,j} = \frac{c_s k_v}{4\Delta r}\left[(r_{j+1/2})^4 - (r_{j-1/2})^4\right]\left\{-G_{j+1/2}\left[f_j + \frac{\Delta r}{2}(f_r)_j\right] + G_{j-1/2}\left[f_{j-1} + \frac{\Delta r}{2}(f_r)_{j-1}\right] + \underbrace{B}_{j=0}\right\} \quad \text{(A7)}$$

where k_v is the volumetric shape factor and the cell-averaged crystal mass is evaluated as

$$f_{w,j} = c_s k_v \int_{r_{j-1/2}}^{r_{j+1/2}} r^3 f_j \, dr = \frac{c_s k_v f_j}{4}((r_{j+1/2})^4 - (r_{j+1/2})^4) \quad \text{(A8)}$$

where f_j is the average population density in the jth cell. The derivatives, $(f_r)_j$, are approximated by the minmod limiter.[30] The solute mass balance can be obtained by summing eq A7 for $j = 0, \ldots, N$. The number of cells, N, was selected to be large enough that $f_{w,N} = 0$ throughout the simulations. Equation A7 and the solute and total mass balance equations, with the nucleation and growth kinetics, were solved with the ODE solver in Matlab 6.5 to obtain the cell-averaged population density function as a function of time.

References

(1) Yu, L. X.; Lionberger, R. A.; Raw, A. S.; D'Costa, R.; Wu, H. Q.; Hussain, A. S. *Adv. Drug Delivery Rev.* **2004**, *56*, 349−369.
(2) Togkalidou, T.; Tung, H. H.; Sun, Y.; Andrews, A. T.; Braatz, R. D. *Ind. Eng. Chem. Res.* **2004**, *43*, 6168−6181.
(3) Worlitschek, J.; Mazzotti, M. *Cryst. Growth Des.* **2004**, *4*, 891−903.
(4) Miller, S. M.; Rawlings, J. B. *AIChE J.* **1994**, *40*, 1312−1327.
(5) Fujiwara, M.; Chow, P. S.; Ma, D. L.; Braatz, R. D. *Cryst. Growth Des.* **2002**, *2*, 363−370.
(6) Gron, H.; Borissova, A.; Roberts, K. J. *Ind. Eng. Chem. Res.* **2003**, *42*, 198−206.
(7) Feng, L. L.; Berglund, K. A. *Cryst. Growth Des.* **2002**, *2*, 449−452.
(8) Liotta, V.; Sabesan, V. *Org. Process Res. Dev.* **2004**, *8*, 488−494.
(9) Fujiwara, M.; Nagy, Z. K.; Chew, J. W.; Braatz, R. D. *J. Process Control* **2005**, *15*, 493−504.
(10) Parsons, A. R.; Black, S. N.; Colling, R. *Chem. Eng. Res. Des.* **2003**, *81*, 700−704.
(11) Barrett, P.; Glennon, B. *Trans. Inst. Chem. Eng.* **2002**, *80*, 799−805.
(12) Wang, F.; Berglund, K. A. *Ind. Eng. Chem. Res.* **2000**, *39*, 2101−2104.
(13) Pollanen, K.; Hakkinen, A.; Reinikainen, S. P.; Louhi-Kultanen, M.; Nystrom, L. *Chemom. Intell. Lab. Syst.* **2005**, *76*, 25−35.
(14) Fevotte, G. *Int. J. Pharm.* **2002**, *241*, 263−278.
(15) Togkalidou, T.; Tung, H.-H.; Sun, Y.; Andrews, A.; Braatz, R. D. *Org. Process Res. Dev.* **2002**, *6*, 317−322.
(16) Togkalidou, T.; Fujiwara, M.; Patel, S.; Braatz, R. D. *J. Cryst. Growth* **2001**, *231*, 534−543.
(17) Fujiwara, M.; Kee, N.; Woo, X. Y.; Wubben, T.; Tan, R. B. H.; Braatz, R. D. *Proceedings of the 2005 American Institute of Chemical Engineers Annual Meeting*; Cincinnati, OH, AIChE Press: New York, Paper 394g.
(18) Henson, M. A., Seborg, D. E., Eds. *Nonlinear Process Control*; Prentice Hall: Piscataway, NJ, 1996.
(19) Ogunnaike, B. A.; Ray, W. H. *Process Dynamics, Modeling, and Control*; Oxford University Press: Oxford, U.K., 1994.
(20) Mullin, J. W.; Nývlt, J. *Chem. Eng. Sci.* **1971**, *26*, 369−377.
(21) Jones, A. G.; Mullin, J. W. *Chem. Eng. Sci.* **1974**, *29*, 105−118.
(22) Mullin, J. W. *Crystallization*, 4th ed.; Elsevier: Amsterdam, 2001.

(23) Borissova, A.; Dashova, Z.; Lai, X.; Roberts, K. J. *Cryst. Growth Des.* **2004**, *3*, 1053−1060.
(24) Uusi-Pentilla, M. S.; Berglund, K. A. In *Crystal Growth of Organic Materials 4*; Ulrich, J., Ed.; Shaker Verlag: Germany, 1997; pp 245−252.
(25) Gabas, N.; Laguerie, C. *Chem. Eng. Sci.* **1992**, *47*, 3148−3152.
(26) Granberg, R. A.; Bloch, D. G.; Rasmuson, A. C. *J. Cryst. Growth* **1999**, *198/199*, 1287−1293.
(27) Granberg, R. A.; Ducreux, C.; Gracin, S.; Rasmuson, A. C. *Chem. Eng. Sci.* **2001**, *56*, 2305−2313.
(28) Randolph, A.; Larson, M. A. *Theory of Particulate Processes*; Academic Press: San Diego, CA, 1988.
(29) Hulburt, H. M.; Katz, S. *Chem. Eng. Sci.* **1964**, *19*, 555−574.
(30) Kurganov, A.; Tadmor, E. *J. Comput. Phys.* **2000**, *160*, 241−282.

CG0504049